

Electronic Supporting Information

for

Synthesis and characterisation of p-block complexes of biquinoline at different ligand charge states

Juha Hurmalainen,^a Akseli Mansikkamäki,^a Ian S. Morgan,^a Anssi Peuronen,^a and Heikki M. Tuononen^{a,*}

^a *University of Jyväskylä, Department of Chemistry, Nanoscience Centre, P.O. Box 35, FI-40014, University of Jyväskylä, Finland.*

E-mail: heikki.m.tuononen@jyu.fi; Tel: +358-40-805-3713

Table of Contents:

Experimental Details	S2
Computational Details	S3
NMR Spectroscopy	S4
IR Spectroscopy	S5
EPR Spectroscopy	S6
Cyclic Voltammetry	S7
X-Ray Crystallography	S8
Theoretical Calculations	S13
References	S16

Experimental Details

All reactions and manipulations were carried out under dry argon atmosphere. Reagents were purchased from Sigma-Aldrich and used as received. All solvents were dried prior to use. Elemental analyses were performed with Vario EL III element analyser.

1: 0.40 g (1.56 mmol) of 2,2'-biquinoline was dissolved in 30 ml of CH₂Cl₂ and cooled to -78°C. The solution was stirred rapidly and 1.56 ml of BCl₃ (1M solution in heptane, 1.56 mmol) was added dropwise. The reaction mixture was gradually brought to 25°C. After stirring for 20 h, the solution had turned yellow and large amounts of yellow precipitate had formed. The solution was filtered off and the solvent was removed under reduced pressure to afford a yellow solid (yield 0.581 g, 1.56 mmol, ≈100 %). ¹H NMR (CD₃CN, 300 MHz, δ ppm): 8.92 (d, 2H, *J* = 8.67 Hz), 8.60 (d, 2H, *J* = 8.61 Hz), 8.41 (d, 2H, *J* = 8.78 Hz), 8.06 (d, 2H, *J* = 8.13 Hz), 7.89 (t, 2H, *J* = 6.91 Hz), 7.72 (t, 2H, *J* = 7.51 Hz). ¹¹B NMR (CD₃CN, 96.25 MHz, δ ppm): 6.88. Elemental analysis (%): calculated: C 57.89 H 3.24 N 7.50; found: C 58.08, H 3.28 N 7.70.

Small amount of **1** was dissolved in acetonitrile and the sealed vessel was placed in a -20°C freezer for a few days to give pale yellow crystals suitable for single crystal X-ray analysis.

2: 25 ml of THF was added to a mixture of **1** (0.25 g, 0.67 mmol) and extremely finely sliced lithium metal (0.005 g, 0.72 mmol). Upon stirring at 25°C, the reaction mixture turned to dark brown. Stirring was continued for 4 h at which point the solution was completely black and no visible traces of lithium could be seen. The solvent was removed under reduced pressure to afford a blackish solid which was redissolved in 15 ml of CH₂Cl₂. After stirring for 10 min, the side product LiCl was filtered off and the solvent removed *in vacuo* to give **2** as a black solid (yield 0.185 g, 0.55 mmol, 82 %). Despite numerous attempts, satisfactory elemental analysis of **2** could not be obtained due to its extreme sensitivity.

Small amount of **2** was dissolved in CH₂Cl₂ and *n*-hexane was carefully layered on top of the solution. The sealed vessel was placed in a -20°C freezer in a glove box for a few days to give extremely air and moisture sensitive dark yellow crystals suitable for single crystal X-ray analysis.

Computational Details

Density functional theory: All density functional theory (DFT) calculations were carried out with the Gaussian 09 program¹ using the PBE1PBE hybrid exchange-correlation functional² and Ahlrichs' TZVP basis sets.³ The geometry of **2** was fully optimized and a frequency calculation was carried out to ensure that the obtained stationary point corresponds to a minimum on the potential energy hypersurface.

Exchange coupling constants between adjacent radicals in the crystal structure geometry of **2** were calculated using the broken symmetry (BS) DFT formalism.⁴ All calculated solutions were subjected to stability analyses to ensure that the self-consistent field procedure has converged to a true minimum on the orbital coefficient hypersurface.⁵ For each radical pair, two states with $MS = 1$ (high-spin, HS) and $MS = 0$ (low-spin, LS) were calculated. The exchange coupling constants were then extracted from the energy difference between these states by interpreting them as Ising states and the respective energies as the energy expectation values of the Heisenberg-Dirac-van Vleck Hamiltonian, $J = 2(E_{LS} - E_{HS})$.⁶

Wave function methods: Multireference calculations on $\text{Co}(\text{biq})_2$ were carried out using the Orca 3.0.3 program package.⁷ First, a state-averaged complete active space (SA-CASSCF) calculation was carried out on the system.⁸ The active space consisted of five Co *d*-orbitals and the HOMOs and LUMOs of both ligands, giving 13 electrons in 9 orbitals. The calculation included 28 lowest roots (7 sextets, 14 quartets, and 7 doublets), which correspond to the CI space formed by coupling the ⁴D term of the Co(II) ion to two ligand doublets.

The size of the active space allows the inclusion of all relevant static correlation effects as well as dynamic correlation arising from ligand-to-metal, metal-to-ligand, and ligand-to-ligand charge transfer (LMCT, MLCT, and LLCT) configurations. The remaining dynamic electron correlation was taken into account using the strongly contracted variant of the second order *N*-electron valence state perturbation theory (NEVPT2).⁹

Scalar relativistic effects were treated through the one-electron operator by using the second order Douglas-Kroll-Hess (DKH) transformation as implemented in Orca.¹⁰ For this reason, the SA-CASSCF and NEVPT2 calculations employed the DKH variants of original def2-TZVP basis sets that have their contraction coefficients re-optimized for relativistic calculations.¹¹ The resolution of identity approximation was used to speed up all integral transformations with the help of auxiliary def2-TZVP/JK basis set.¹²

NMR Spectroscopy

NMR spectra of **1** were measured at 25°C using a Bruker Avance 300 MHz spectrometer.

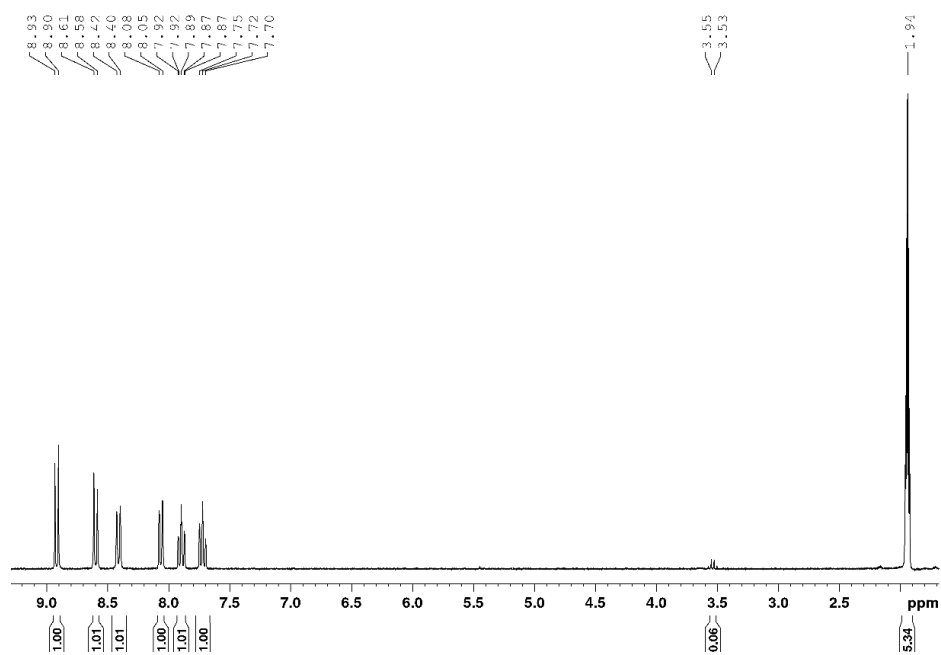


Figure S1. ^1H NMR spectrum of **1** in CD_3CN .

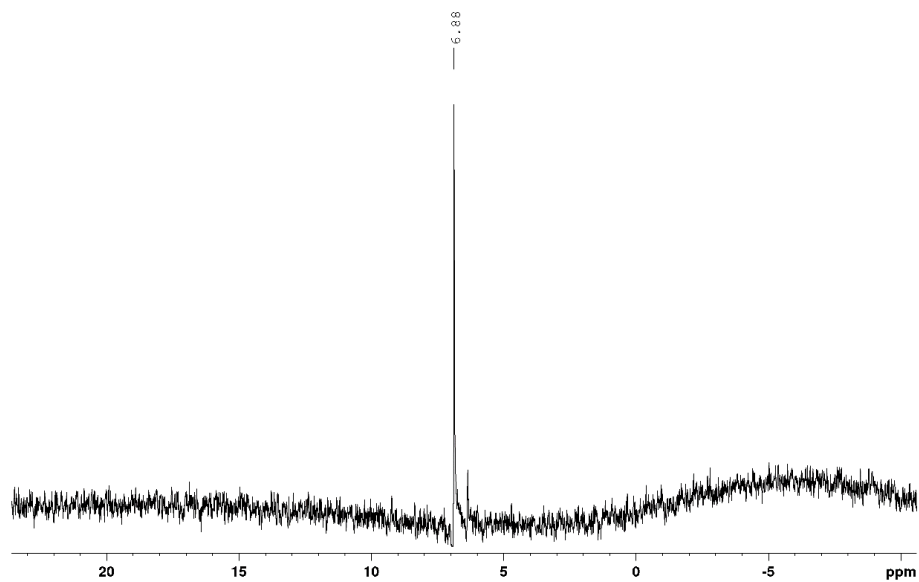


Figure S2. ^{11}B NMR spectrum of **1** in CD_3CN .

IR Spectroscopy

IR spectrum of **1** was measured at 25°C using a Bruker ALPHA FT-IR spectrometer.

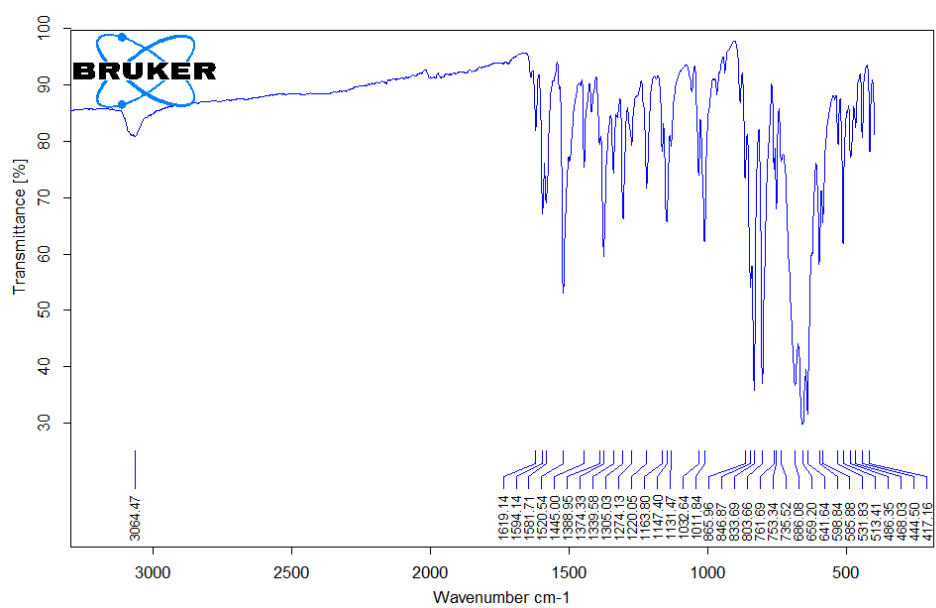


Figure S3. IR spectrum of **1**.

EPR Spectroscopy

EPR spectrum of **2** was recorded at 25°C using Magnettech GmbH MiniScope 200 X-band EPR spectrometer. Simulation of the spectral data was done using EasySpin software.¹³

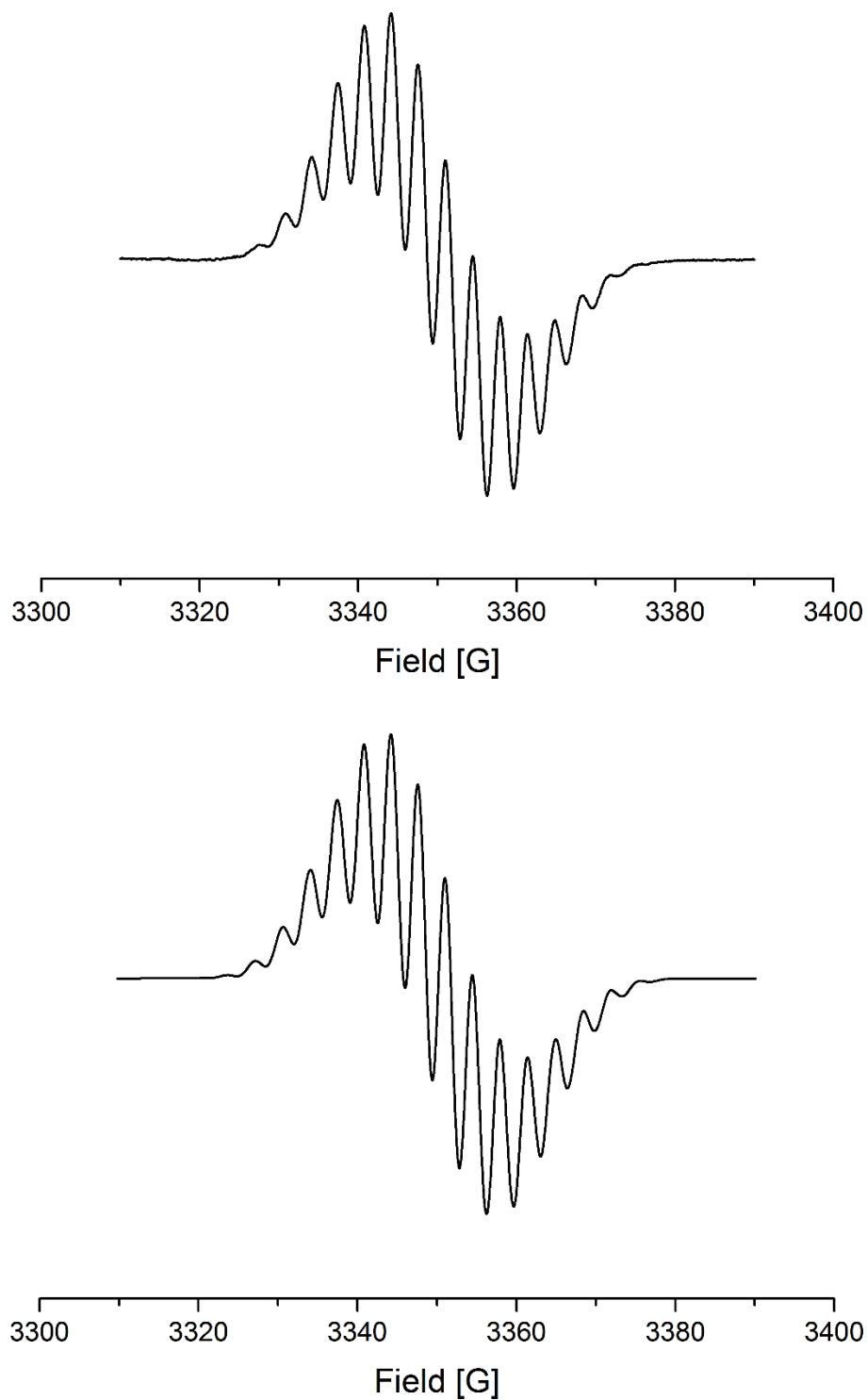


Figure S4. EPR spectrum of **2** in CH_2Cl_2 (top) and its simulation (bottom).

Cyclic Voltammetry

Cyclic voltammogram of **1** was measured at 25°C using a BASi Epsilon potentiostat with scans of 100 mV/s. A degassed CH₃CN solution of **1** containing 0.1 M of [(*n*-Bu)₄N][PF₆] as the supporting electrolyte was used. Potentials were scanned with respect to a quasi-reference electrode in a single compartment cell fitted with Pt electrodes and referenced to Fc/Fc⁺ couple (vs. SCE).

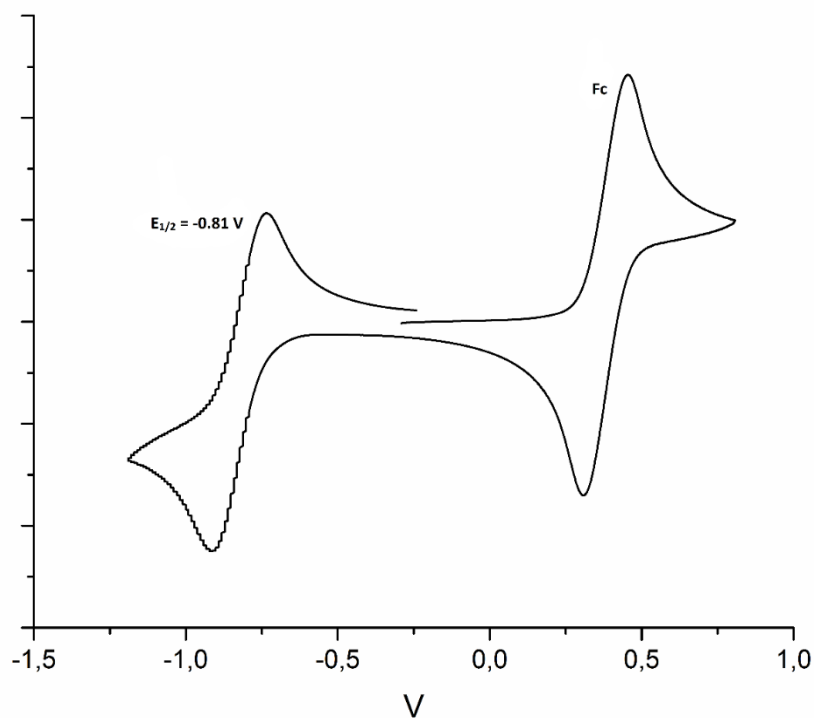


Figure S5. Cyclic voltammogram of **1** in CH₃CN.

X-Ray Crystallography

Single crystal data of **1** and **2** were collected at -150°C with Agilent Technologies SuperNova diffractometer equipped with a multilayer optics monochromated dual source (Cu and Mo) Atlas detector and using $\text{CuK}\alpha$ (1.54184 \AA) radiation. CrystalsPro was used for data acquisition, reduction, and analytical face-index based absorption correction.¹⁴ Structures were solved with the ShelXT program and refined on F^2 by full matrix least squares method using the ShelXL program.¹⁵ Olex² software was used throughout the process of solving and refining the structures.¹⁶ Hydrogen atoms were treated as riding atoms using U_{iso} parameters of 1.2 times that of the host atom.

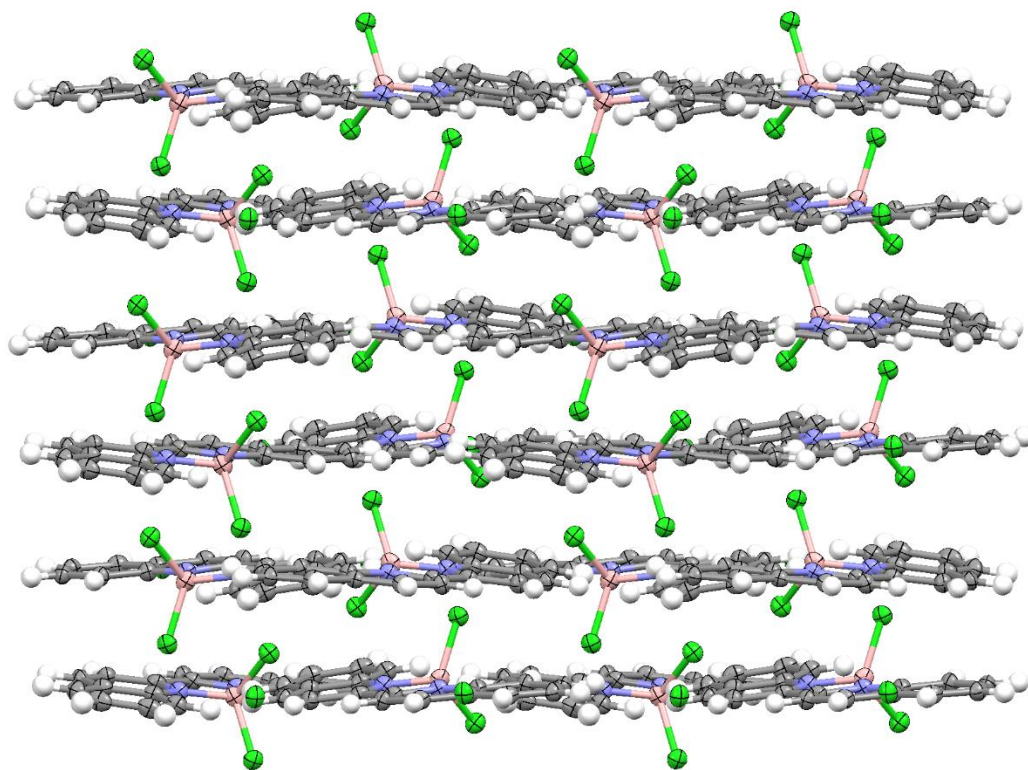


Figure S6. Layer-like packing of **1** in the solid state.

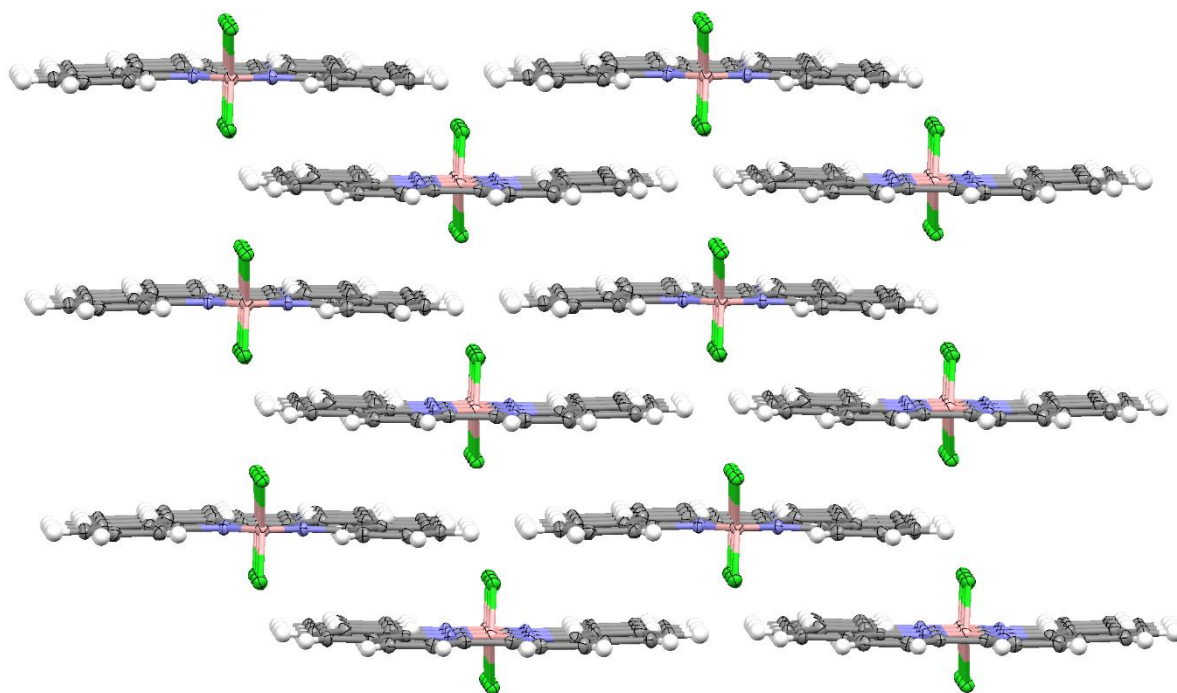


Figure S7. Layered packing of **2** in the solid state.

Table S1. Crystallographic data for compounds **1** and **2**.

	1	2
Empirical formula	C ₁₈ H ₁₂ BN ₂ Cl ₃	C ₁₈ H ₁₂ BCl ₂ N ₂
Formula weight	373.46	338.01
Temperature [K]	123.00(10)	123.00(10)
Crystal system	monoclinic	triclinic
Space group	P2 ₁ /n	P-1
<i>a</i> [Å]	9.8065(6)	6.7519(13)
<i>b</i> [Å]	11.7319(7)	7.7698(14)
<i>c</i> [Å]	14.6860(12)	14.179(3)
α [°]	90	86.739(15)
β [°]	107.874(8)	86.016(15)
γ [°]	90	86.206(15)
Volume [Å ³]	1608.1(2)	739.4(2)
<i>Z</i>	4	2
ρ_{calc} [g cm ⁻³]	1.543	1.518
μ [mm ⁻¹]	5.16	3.92
<i>F</i> (000)	760	346
Crystal size [mm ³]	0.112 × 0.039 × 0.022	0.128 × 0.03 × 0.019
Radiation	CuK α (λ = 1.54184)	CuK α (λ = 1.54184)
2 θ range for data collection [°]	9.646 to 137.99	11.43 to 137.996
Index ranges	-11 ≤ <i>h</i> ≤ 8, -14 ≤ <i>k</i> ≤ 13, -15 ≤ <i>l</i> ≤ 17	-8 ≤ <i>h</i> ≤ 8, -9 ≤ <i>k</i> ≤ 9, -17 ≤ <i>l</i> ≤ 8
Reflections collected	5078	4291
Independent reflections	2959 [<i>R</i> _{int} = 0.0401, <i>R</i> _{σ} = 0.0672]	2698 [<i>R</i> _{int} = 0.0514, <i>R</i> _{σ} = 0.0787]
Data/restraints/parameters	2959/0/217	2698/0/208
Goodness-of-fit on <i>F</i> ²	1.036	1.038
Final <i>R</i> indexes [<i>I</i> ≥ 2 σ (<i>I</i>)]	<i>R</i> ₁ = 0.0473, <i>wR</i> ₂ = 0.1111	<i>R</i> ₁ = 0.0603, <i>wR</i> ₂ = 0.1567
Final <i>R</i> indexes [all data]	<i>R</i> ₁ = 0.0662, <i>wR</i> ₂ = 0.1211	<i>R</i> ₁ = 0.0786, <i>wR</i> ₂ = 0.1690
Largest diff. peak/hole [e Å ⁻³]	0.42/-0.47	1.44/-0.34

Table S2. Bond lengths (Å) of compounds **1** and **2**.

1		2	
Cl2 - B1	1.820(4)	Cl1 - B1	1.863(4)
Cl1 - B1	1.846(4)	Cl2 - B1	1.874(4)
N1 - C1	1.377(4)	N1 - C1	1.394(5)
N1 - C9	1.342(4)	N1 - C9	1.380(5)
N1 - B1	1.566(5)	N1 - B1	1.536(5)
N2 - C10	1.346(4)	N2 - C10	1.373(5)
N2 - C18	1.368(4)	N2 - C18	1.390(5)
N2 - B1	1.565(4)	N2 - B1	1.541(5)
C10 - C9	1.456(5)	C1 - C2	1.398(6)
C10 - C11	1.407(4)	C1 - C6	1.421(5)
C13 - C14	1.411(5)	C2 - C3	1.387(5)
C13 - C12	1.411(5)	C3 - C4	1.404(6)
C13 - C18	1.431(4)	C4 - C5	1.364(6)
C14 - C15	1.364(5)	C5 - C6	1.406(5)
C12 - C11	1.367(5)	C6 - C7	1.425(6)
C2 - C1	1.410(5)	C7 - C8	1.370(6)
C2 - C3	1.374(5)	C8 - C9	1.403(5)
C1 - C6	1.418(5)	C9 - C10	1.411(5)
C9 - C8	1.394(5)	C10 - C11	1.404(5)
C15 - C16	1.415(5)	C11 - C12	1.371(6)
C8 - C7	1.373(5)	C12 - C13	1.431(6)
C3 - C4	1.402(6)	C13 - C14	1.406(5)
C5 - C6	1.414(5)	C13 - C18	1.424(5)
C5 - C4	1.370(5)	C14 - C15	1.376(6)
C17 - C18	1.407(5)	C15 - C16	1.397(6)
C17 - C16	1.365(5)	C16 - C17	1.385(5)
C7 - C6	1.414(5)	C17 - C18	1.398(5)

Table S3. Bond angles (°) of compounds **1** and **2**.

1		2	
C1 - N1 - B1	127.4(3)	C1 - N1 - B1	128.9(3)
C9 - N1 - C1	121.6(3)	C9 - N1 - C1	121.1(3)
C9 - N1 - B1	110.9(3)	C9 - N1 - B1	110.0(3)
C10 - N2 - C18	122.2(3)	C10 - N2 - C18	121.0(3)
C10 - N2 - B1	110.3(3)	C10 - N2 - B1	110.0(3)
C18 - N2 - B1	127.5(3)	C18 - N2 - B1	129.0(3)
N2 - C10 - C9	110.4(3)	N1 - C1 - C2	121.5(3)
N2 - C10 - C11	122.0(3)	N1 - C1 - C6	118.5(3)
C11 - C10 - C9	127.6(3)	C2 - C1 - C6	120.0(3)
C14 - C13 - C18	118.8(3)	C3 - C2 - C1	119.4(4)
C12 - C13 - C14	122.5(3)	C2 - C3 - C4	120.9(4)
C12 - C13 - C18	118.8(3)	C5 - C4 - C3	119.7(4)
C15 - C14 - C13	119.9(3)	C4 - C5 - C6	121.3(4)
C11 - C12 - C13	121.7(3)	C1 - C6 - C7	119.2(3)
C3 - C2 - C1	118.9(4)	C5 - C6 - C1	118.6(4)
N1 - C1 - C2	121.4(3)	C5 - C6 - C7	122.3(4)
N1 - C1 - C6	118.0(3)	C8 - C7 - C6	121.1(4)
C2 - C1 - C6	120.6(3)	C7 - C8 - C9	118.9(4)
N1 - C9 - C10	109.6(3)	N1 - C9 - C8	121.2(3)
N1 - C9 - C8	122.7(3)	N1 - C9 - C10	110.0(3)
C8 - C9 - C10	127.7(3)	C8 - C9 - C10	128.8(3)
C14 - C15 - C16	120.7(3)	N2 - C10 - C9	110.1(3)
C7 - C8 - C9	117.2(3)	N2 - C10 - C11	121.4(3)
C2 - C3 - C4	121.1(3)	C11 - C10 - C9	128.5(4)
C4 - C5 - C6	120.1(4)	C12 - C11 - C10	119.1(4)
C16 - C17 - C18	119.1(3)	C11 - C12 - C13	120.8(3)
C12 - C11 - C10	117.4(3)	C14 - C13 - C12	122.3(3)
N2 - C18 - C13	117.9(3)	C14 - C13 - C18	118.9(4)
N2 - C18 - C17	121.9(3)	C18 - C13 - C12	118.8(3)
C17 - C18 - C13	120.2(3)	C15 - C14 - C13	120.7(3)
C8 - C7 - C6	121.5(3)	C14 - C15 - C16	120.2(4)
C5 - C6 - C1	118.6(3)	C17 - C16 - C15	120.5(4)
C7 - C6 - C1	118.9(3)	C16 - C17 - C18	120.2(4)
C7 - C6 - C5	122.5(3)	N2 - C18 - C13	118.9(3)
C17 - C16 - C15	121.2(3)	N2 - C18 - C17	121.5(3)
Cl2 - B1 - Cl1	112.8(2)	C17 - C18 - C13	119.6(3)
N1 - B1 - Cl2	111.9(3)	Cl1 - B1 - Cl2	109.9(2)
N1 - B1 - Cl2	110.2(2)	N1 - B1 - Cl1	112.2(2)
N2 - B1 - Cl2	113.2(3)	N1 - B1 - Cl2	111.5(3)
N2 - B1 - Cl1	109.2(3)	N1 - B1 - N2	99.9(3)
N2 - B1 - N1	98.7(3)	N2 - B1 - Cl1	112.1(3)
C5 - C4 - C3	120.8(3)	N2 - B1 - Cl2	111.0(2)

Theoretical Calculations

Calculated hyperfine coupling constants. Hyperfine coupling constants were calculated for **2** in its optimized geometry using the PBE1PBE/TZVP method. The results show coupling of the unpaired electron primarily to one boron (^{11}B ; -4.59 G), two nitrogen (^{14}N ; 2.41 G), two chlorine (^{35}Cl ; 2.46 G), and two hydrogen (^1H ; -3.58 G) nuclei with smaller couplings to three pairs of equivalent hydrogen (^1H ; -1.04 , 1.01 , and -0.85 , G) centres and only minute couplings to the remaining two pairs of equivalent hydrogen atoms (^1H ; -0.41 and -0.27 G).

Intermolecular exchange interactions in **2.** Exchange coupling constants (J) between adjacent (nearest neighbour) radicals in the crystal structure of **2** were calculated using the BS-PBE1PBE/TZVP method. The results show that the exchange coupling mediated by π -stacking interactions along the crystallographic a -axis is weak but not negligible, $J_a = -41.6$ cm^{-1} (-0.50 kJ mol^{-1}). The coupling along the crystallographic b -axis is more than an order of magnitude smaller, $J_b = 1.3$ cm^{-1} (0.02 kJ mol^{-1}) and below any reasonable margin of error in DFT calculations. The coupling constant calculated for the exchange interaction along the crystallographic c -axis, J_c , was even smaller and cannot be separated from numerical noise.

The reason why the exchange coupling mediated by π -stacking interactions is weak can be understood by looking at the SOMO...SOMO interactions along the crystallographic a -axis. In the crystal structure geometry, the two interacting SOMOs are almost orthogonal due to their matching nodal properties. Hence, the radicals **2** can pack closely without forming π -dimers. This was tested computationally by calculating the coupling constant J_a using the crystal structure geometry but bringing the two radicals significantly closer to each other. When the radical...radical distance was decreased from *ca.* 3.4 Å (crystal structure) to 3.0 Å, the coupling constant decreased to -101.1 cm^{-1} (-1.21 kJ mol^{-1}). For comparison, the experimental coupling constant between two 2,5,8-tri-*tert*-butylphenalenyl radicals in the π -dimer geometry (radical...radical distance *ca.* 3.29 Å) is -1390 cm^{-1} (-16.63 kJ mol^{-1}).

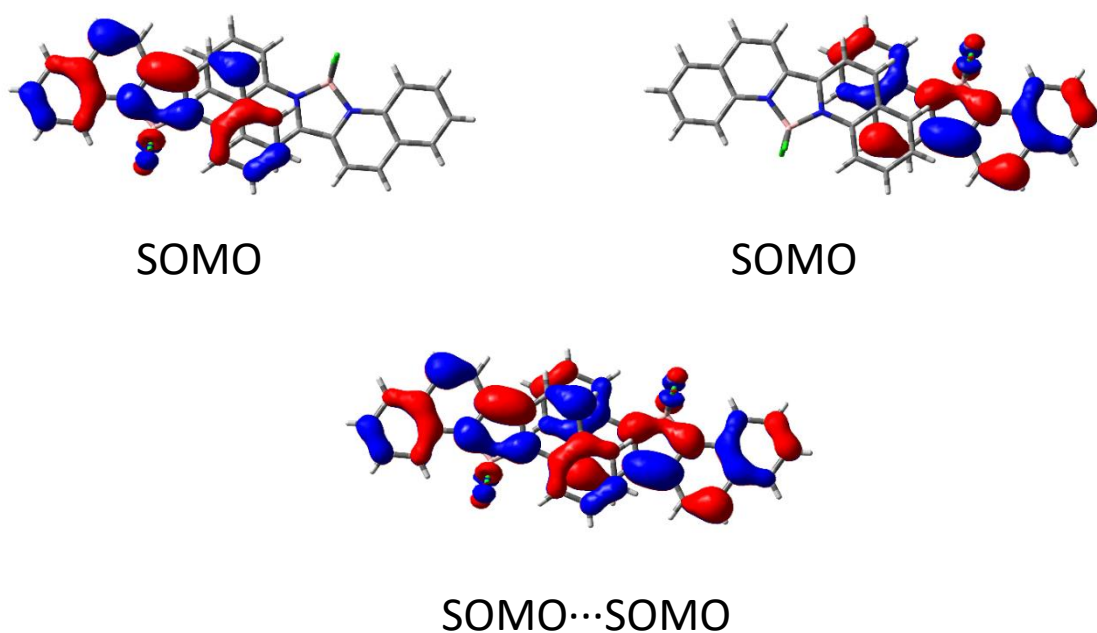


Figure S8. Nearly orthogonal SOMO...SOMO interactions in the solid state structure of **2** (along the crystallographic a -axis).

The electronic structure of Co(biq)₂. The electronic structure of Co(biq)₂ was analysed using multireference electron correlation methods (DKH-NEVPT2/DKH-SA-CASSCF(13,9)/def2-TZVP). Energies and multiplicities of the 28 lowest states of the complex are given in Table S1 along with the relative contributions (%) from different classes of electronic configurations to the wave functions. In all cases, the listed contributions account more than 96% of the total wave function.

The results show that the ground state of Co(biq)₂ is a spin-doublet. The lowest eight states, consisting of two doublets, four quartets, and two sextets, form a manifold which is separated from the higher-lying states by 4862 cm⁻¹. This manifold corresponds to the set of electronic states that are formed by exchange mixing of the two lowest crystal field states of quartet Co(II) ion with the two ligand radical doublets. Based on the energetic ordering of different multiplicities, the dominant components of exchange interactions are antiferromagnetic.

Around 60% of the ground state wave function consists of electronic configurations corresponding to a high-spin Co(II) ion and two anionic radical ligands. The other two classes contributing to the ground state wave function are LMCT and MLCT configurations with contributions of 26% and 8%, respectively. Based on these observations, the ground state of Co(biq)₂ can be viewed as an antiferromagnetically coupled high-spin Co(II) ion and two anionic radical ligands, stabilized by significant kinetic exchange.

An investigation of the wave functions of other states given in Table 1 reveals clear trends. The sum of Co(II) configurations is in all cases at least 60%, but LMCT and MLCT configurations, corresponding to a Co(I) ion, also make significant (up to 34%) contributions to all doublet and quartet states. This applies especially to the lowest states of Co(biq)₂, including its ground state. The sextet states are in all cases dominated by the configuration corresponding to a high-spin Co(II) ion and two anionic radical ligands (more than 96%). It should also be noted that the contribution of the double LMCT configuration, corresponding to a Co(0) ion, is at most 3%. Thus, there is no justification for identifying the Co charge state as zero in any of the states, including the ground state of Co(biq)₂.

Table S4. Analysis of wave functions corresponding to the 28 lowest states of the complex $\text{Co}(\text{biq})_2$.^a

State	2S+1	Relative energy [cm ⁻¹]	Relative contribution [%]						Sum
			Co(II)		Co(I)	Co(III)	Co(0)	Co(IV)	
			Co ^{II} (biq [*]) ₂	LLCT	LMCT	MLCT	Double LMCT	Double MLCT	
0	2	0	60.27	0.80	26.16	7.95	3.06	0.27	98.50
1	2	1437	59.95	0.74	26.23	7.94	3.14	0.27	98.28
2	4	1756	73.40	0.00	19.50	5.99	0.00	0.00	98.89
3	4	2626	0.00	81.78	12.70	3.89	0.00	0.00	98.36
4	4	3150	72.99	0.00	19.73	5.96	0.00	0.00	98.67
5	4	3998	0.00	81.61	12.91	3.87	0.00	0.00	98.38
6	6	4149	99.91	0.00	0.00	0.00	0.00	0.00	99.91
7	6	5497	99.67	0.00	0.00	0.00	0.00	0.00	99.67
8	2	10359	71.42	0.00	18.02	7.69	0.00	0.00	97.13
9	4	10624	61.63	14.54	14.65	6.12	0.00	0.00	96.95
10	4	10989	24.64	54.33	12.60	5.73	0.00	0.00	97.30
11	4	11248	45.72	28.95	16.36	6.73	0.00	0.00	97.74
12	4	11398	35.44	39.80	16.19	6.17	0.00	0.00	97.60
13	2	11634	73.62	0.00	15.97	7.40	0.00	0.00	96.98
14	2	11718	70.13	0.26	17.63	7.31	1.81	0.00	97.14
15	2	11791	73.85	0.00	15.94	7.87	0.00	0.00	97.66
16	6	12297	96.76	0.00	0.00	2.76	0.00	0.00	99.52
17	4	12448	45.06	42.14	6.62	3.52	0.00	0.00	97.34
18	2	12493	74.74	0.00	15.61	7.55	0.00	0.00	97.91
19	4	12985	31.13	58.75	4.10	3.65	0.00	0.00	97.63
20	6	13019	96.37	0.00	0.00	3.24	0.00	0.00	99.61
21	4	13172	69.83	12.03	10.58	5.15	0.00	0.00	97.59
22	6	13336	96.44	0.00	0.00	2.61	0.00	0.00	99.05
23	4	13681	6.32	80.08	6.97	4.36	0.00	0.00	97.73
24	6	13814	96.44	0.00	0.00	2.83	0.00	0.00	99.28
25	4	14003	44.11	49.77	0.26	2.83	0.00	0.00	96.96
26	4	14200	43.03	50.23	1.03	2.83	0.00	0.00	97.12
27	6	14544	97.13	0.00	0.00	2.51	0.00	0.00	99.64

^a Configurations with contributions smaller than 0.25% have been excluded. LLCT = ligand-to-ligand charge transfer; LMCT = ligand-to-metal charge transfer; MLCT = metal-to-ligand charge transfer.

References

- ¹ Gaussian 09, Revision D.01, M. J. Frisch, G. W. Trucks, H. B. Schlegel, G. E. Scuseria, M. A. Robb, J. R. Cheeseman, G. Scalmani, V. Barone, B. Mennucci, G. A. Petersson, H. Nakatsuji, M. Caricato, X. Li, H. P. Hratchian, A. F. Izmaylov, J. Bloino, G. Zheng, J. L. Sonnenberg, M. Hada, M. Ehara, K. Toyota, R. Fukuda, J. Hasegawa, M. Ishida, T. Nakajima, Y. Honda, O. Kitao, H. Nakai, T. Vreven, J. A. Montgomery, Jr., J. E. Peralta, F. Ogliaro, M. Bearpark, J. J. Heyd, E. Brothers, K. N. Kudin, V. N. Staroverov, R. Kobayashi, J. Normand, K. Raghavachari, A. Rendell, J. C. Burant, S. S. Iyengar, J. Tomasi, M. Cossi, N. Rega, J. M. Millam, M. Klene, J. E. Knox, J. B. Cross, V. Bakken, C. Adamo, J. Jaramillo, R. Gomperts, R. E. Stratmann, O. Yazyev, A. J. Austin, R. Cammi, C. Pomelli, J. W. Ochterski, R. L. Martin, K. Morokuma, V. G. Zakrzewski, G. A. Voth, P. Salvador, J. J. Dannenberg, S. Dapprich, A. D. Daniels, Ö. Farkas, J. B. Foresman, J. V. Ortiz, J. Cioslowski, D. J. Fox, Gaussian Inc., Wallingford CT, 2009.
- ² (a) C. Adamo, V. Barone, *J. Chem. Phys.*, 1999, **110**, 6158; (b) M. Ernzerhof, G. E. Scuseria, *J. Chem. Phys.*, 1999, **110**, 5029; (c) J. P. Perdew, K. Burke, M. Ernzerhof, *Phys. Rev. Lett.*, 1996, **78**, 1396; (d) J. P. Perdew, K. Burke, M. Ernzerhof, *Phys. Rev. Lett.*, 1996, **77**, 3865
- ³ A. Schäfer, C. Huber, R. Ahlrichs, *J. Chem. Phys.*, 1994, **100**, 5829.
- ⁴ (a) L. Noodleman, E. R. Davidson, *Chem. Phys.*, 1986, **109**, 131; (b) L. Noodleman, J. G. Norman, Jr., J. H. Osborne, A. Aizman, D. A. Case, *J. Am. Chem. Soc.*, 1985, **107**, 3418; (c) G. Jonkers, C. A. Lange, L. Noodleman, E. J. Baerends, *Mol. Phys.*, 1982, **46**, 609; (d) L. Noodleman, *J. Chem. Phys.*, 1981, **74**, 5737.
- ⁵ (a) R. Bauernschmitt, R. Ahlrichs, *J. Chem. Phys.*, 1996, **104**, 9047; (b) R. Seeger, J. A. Pople, *J. Chem. Phys.*, 1977, **66**, 3045.
- ⁶ (a) I. de P. R. Moreira, F. Illas, *Phys. Chem. Chem. Phys.*, 2006, **8**, 1645; (b) D. Dai, M.-H. Whangbo, *J. Chem. Phys.*, 2001, **114**, 2887.
- ⁷ F. Neese, *Wiley Interdiscip. Rev. Comput. Mol. Sci.*, 2012, **2**, 73.
- ⁸ B. O. Roos, in *Advances in Chemical Physics, Ab Initio Methods in Quantum Chemistry II*, Vol. 69 (Ed.: K. P. Lawley), Wiley, New York, 1987, pp. 399–455.
- ⁹ (a) C. Angeli, C. Cimiraglia, J.-P. Malrieu, *J. Chem. Phys.*, 2002, **117**, 9138; (b) C. Angeli, R. Cimiraglia, S. Evangelisti, T. Leininger, J.-P. Malrieu, *J. Chem. Phys.*, 2001, **114**, 10252; (c) C. Angeli, C. Cimiraglia, J.-P. Malrieu, *Chem. Phys. Lett.*, 2001, **350**, 297.
- ¹⁰ (a) B. A. Hess, *Phys. Rev. A*, 1986, **3**, 3742; (b) M. Douglas, N. M. Kroll, *Ann. Phys.*, 1974, **82**, 89.
- ¹¹ (a) D. A. Pantazis, X. Y. Chen, C. R. Landis, F. Neese, *J. Chem. Theory Comput.*, 2008, **4**, 908; (b) F. Weigend, R. Ahlrichs, *Phys. Chem. Chem. Phys.*, 2005, **7**, 3297.
- ¹² F. Weigend, *J. Comp. Chem.*, 2008, **29**, 167.
- ¹³ S. Stoll, A. Schweiger, *J. Magn. Reson.*, 2006, **178**, 42.
- ¹⁴ CrysAlisPro program, version 1.171.36.21, Agilent Technologies, Oxford, 2012.
- ¹⁵ (a) G. M. Sheldrick, *Acta Cryst.*, 2015, **C71**, 3; (b) G. M. Sheldrick, *Acta Cryst.*, 2008, **A64**, 112.
- ¹⁶ O. V. Dolomanov, L. J. Bourhis, R. J. Gildea, J. A. K. Howard, H. J. Puschmann, *J. Appl. Cryst.*, 2009, **42**, 339.
- ¹⁷ Y. Takano, T. Taniguchi, H. Isobe, T. Kubo, Y. Morita, K. Yamamoto, K. Nakasuji, T. Takui, and K. Yamaguchi, *J. Am. Chem. Soc.*, 2002, **124**, 11122.